Indian Journal of Pure & Applied Physics
Vol. 55, August 2017, pp. 595-603

0.5 V log-domain realization of tinnitus detection system

Farooq Ahmad Khanday[a]*, Imran Nazir Beigh[a] & Costas Psychalinos[b]

[a]Department of Electronics and Instrumentation Technology, University of Kashmir, Srinagar 190 006, India

[b]Electronics Laboratory, Physics Department, University of Patras, Rio Patras, GR 26504, Greece

Received 21 July 2016; accepted 14 March 2017

A low-voltage tinnitus detection system using log-domain technique has been introduced in this paper. The design offers the advantages of resistorless design, electronic tunability of performance characteristics, and less complexity than the reported ones. The performance of the tinnitus detector has been verified by HSPICE simulation software using the parameters of TSMC CMOS 130 nm process.

Keywords: Biomedical electronics, Tinnitus, Tinnitus detection system, Low-voltage design, Analog integrated circuits, Companding, Log-domain technique

1 Introduction

Tinnitus (from the Latin *tinnire*, which means to ring or to tinkle) is the perception of sound (of ring, buzz, roar or hiss form) for which there is no evident external stimulus[1,2]. It is the indication of malfunction in the processing of auditory signals involving both perceptual and psychological components. There can be many possible causes for tinnitus including exposure to loud sounds, injuries to head or neck, reaction to medication, natural aging, sudden impact noises, earwax blockage, and ear bone changes[3]. As far as the treatment of tinnitus is concerned there are a number of therapy procedures such as acupuncture, cranio-sacrat therapy, cognitive therapy behavioral therapy, tinnitus retaining therapy and hypnosis or hyperbaric oxygen[4-6]. Before a patient is treated for tinnitus, it is essential to verify whether a patient suffers from tinnitus or not. Therefore, from the last few years, a considerable attention has been given by the researchers to design a tinnitus detection system[7,8]. The idea behind the designs is to extract the energies corresponding alpha, theta and gamma waves of electroencephalogram (EEG) from healthy and deceased regions of brain and if the extracted energies of theta and gamma waves from deceased region is higher than the healthy region and that of alpha wave is lower than the healthy region, tinnitus is detected.

The designs of tinnitus detection system were introduced keeping in view its employment in closed-loop implantable neuro device for electrical stimulation of deceased areas of auditory cortex. Therefore, low-voltage implementation and low-power dissipation were the main design concerns in its design. Among the several low-voltage techniques, companding is supposed to be the most suitable technique for its design.

In companding[9,10], the large-signal characteristics of MOS transistor are directly used without any additional linearization technique. The input signal is first compressed using an appropriate compressor, the compressed signal is processed by the core of the companding system and then the compressed output of the core is expanded by an appropriate expander. Therefore a companding system forms externally linear internally non-linear (ELIN) system. The three classes of companding systems reported in the open literature are log-domain system[11-16], square-root domain system[17-20] and sinh-domain system[21-26]. Log-domain systems were the most widely studied systems but due to their bipolar implementations, they became obsolete with time and many square-root system implementations were reported. However, square-root system implementations have the limitations of large supply voltage, high complexity and high power dissipation. Therefore, the researchers started to design the sinh-domain systems which offer the advantages of class AB nature and low-power consumption. The sinh-domain system however has the disadvantage of high complexity. Therefore, in the last few years, the researchers have again started to design the CMOS log-domain systems which

*Corresponding author (E-mail: farooqsnn20@yahoo.co.in)

overcome the high-complexity disadvantage of sinh-domain systems.

In this paper, a log-domain tinnitus detection system is presented. Compared to the design proposed by Hiseni *et al.*[7], the proposed design offers the advantages of exact design as the square function has not been approximated and the low supply voltage design. Compared to the design of Tsirimokou *et al.*[8], the proposed design offers the advantages of low complexity and large dynamic range (DR).

2 Tinnitus Detection System

The tinnitus detection system is recalled in Fig. 1, where the signals have been received from the electrodes associated with the healthy and deceased locations of the auditory cortex. There are two energy extractors for each frequency band, i.e., alpha, gamma, and theta which are connected to the deceased and healthy locations, to extract the energy of the signals originated from their auditory cortex, respectively. Each energy extractor consists of a band-pass (BP) filter, a squarer, and a low-pass (LP) filter as shown in Fig. 2. To extract the band of interest from the EEG signal, BP filter is used while as the squarer will perform the full wave rectification of the filtered signal which is fed as input to the LP filter with cut-off frequency much smaller than the maximum frequency of the squarer's output signal.

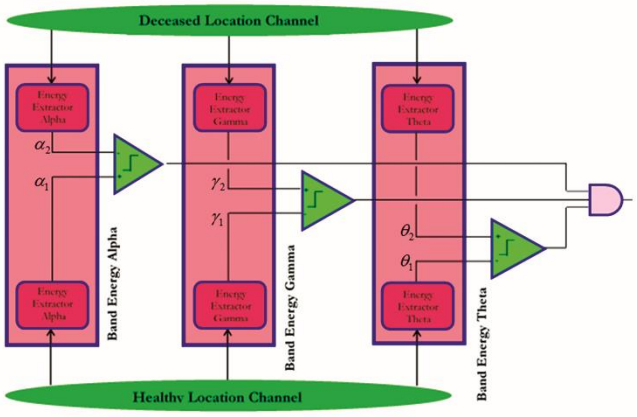

Fig. 1 — Tinnitus detection system.

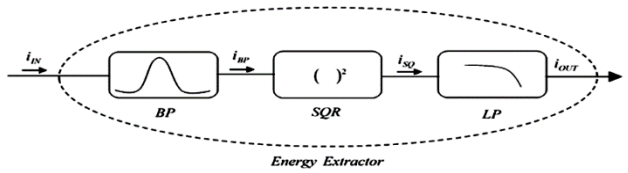

Fig. 2 — Construction of energy extractor using squarer and filter building blocks.

The LP filter therefore provides the information about the energy of the applied input signal. The output of the energy extractors alpha, gamma and theta are denoted by (α_1,α_2), (Υ_1 , Υ_2) and (θ_1 , θ_2) respectively. As shown in Fig. 1, the output of the energy extractors of particular band is fed to the input of corresponding comparator and then comparators are appropriately configured to produce logic 1 at their output. If $\alpha_1>\alpha_2$, $\Upsilon_1<\Upsilon_2$ and $\theta_1<\theta_2$, only then the output of AND gate will be at logic 1 which means tinnitus is diagnosed.

The functional block diagrams (FBDs) employed to implement the second order band-pass and low-pass filters are shown in Figs 3(a) and 3(b), respectively, where the corresponding transfer function are given by Eqs (1) and (2), respectively;

$$H_{BP}(s) = \frac{(\omega_o/Q).s}{s^2+(\omega_o/Q).s+\omega_o^2} \quad \ldots (1)$$

$$H_{LP}(s) = \frac{\omega_o^2}{s^2+(\omega_o/Q).s+\omega_o^2} \quad \ldots (2)$$

where the resonant frequency (ω_o) and quality factor (Q) are given by Eqs (3) and (4), respectively:

$$\omega_o = \frac{1}{\sqrt{\tau_1\tau_2}} \quad \ldots (3)$$

$$Q = \sqrt{\frac{\tau_1}{\tau_2}} \quad \ldots (4)$$

3 Log-Domain Implementation of Tinnitus Detection System

The topology of a log-domain lossless integrator required to implement the filtering functions is shown in Fig. 4. After some algebriac manuplations, the transfer function of the integrator is derived as given in Eq. (5):

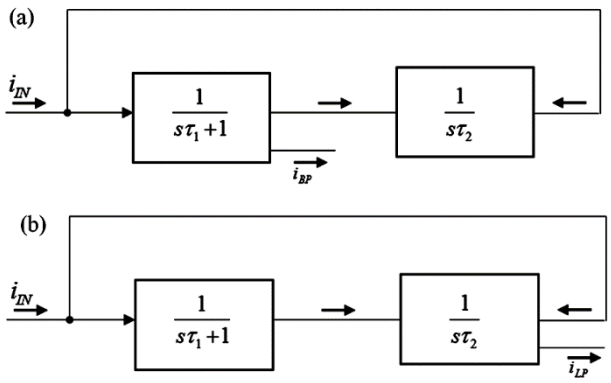

Fig. 3 — FBD of second order (a) band-pass filter and (b) low-pass filter.

$$H(S) = \frac{1}{\hat{\tau} s} \quad \ldots (5)$$

where the time constant $\hat{\tau}$ is given by Eq. (6):

$$\tau = \hat{C} n V_T / I_o \quad \ldots (6)$$

To realize a log-domain integrator *E*+ cell and *E*- cell (i.e., non-linear transconductor cells) are the basic building blocks which are shown in Figs 5 and 6, respectively, and the expression is given by Eq. (7):

$$i_{OUT} = I_o . e^{\frac{\hat{\upsilon}_+ - \hat{\upsilon}_-}{\eta V_T}} \quad \ldots (7)$$

where I_o is dc bias current, V_T is the thermal voltage (26 mV at 27 °C), *n* is the sub threshold slope factor (1< *n* <2), $\hat{\upsilon}_+$, $\hat{\upsilon}_-$ are the compressed input voltages and i_{OUT} is the linear output current.

The complementary operators used to convert the linear input current into a compressed voltage (LOG) and the compressed output voltage into a linear current (EXP) are given in Figs 7(a) and 7(b), respectively. The input-output relationship of LOG and EXP operators is given in Eqs (8) and (9), respectively:

$$\text{LOG}(i_{IN}) = \hat{\upsilon}_{IN} = V_{DC} + \eta V_T . \ln\left(\frac{i_{IN} + I_O}{I_O}\right) \quad \ldots (8)$$

$$\text{EXP}(\hat{v}_{OUT}) = i_{OUT} = I_o . e^{\frac{\hat{\upsilon}_{OUT} - V_{DC}}{\eta V_T}} - I_o \quad \ldots (9)$$

The combined log-domain implementation of second-order band-pass and low-pass filter is shown in Fig. 8.

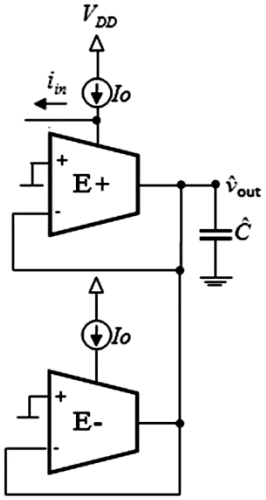

Fig. 4 — Log-domain implementation of lossless integrator.

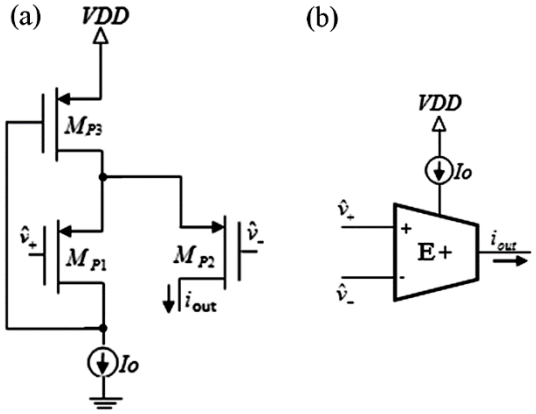

Fig. 5 — Positive transconductance cell (a) transistor level circuit and (b) symbol.

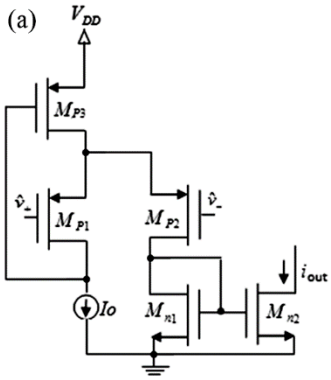

Fig. 6 — Negative transconductance cell (a) transistor level circuit and (b) symbol.

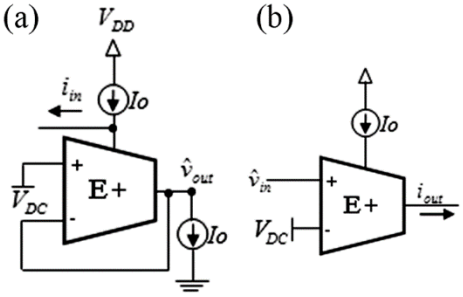

Fig. 7 — (a) Compressor block and (b) expander block.

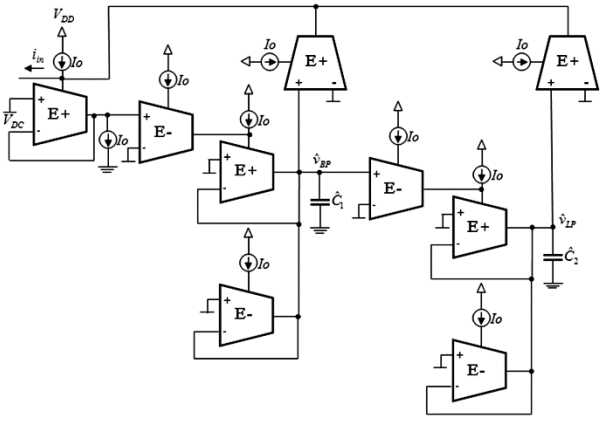

Fig. 8 —Topology of second-order low-pass and band-pass filter.

The resonant frequency ω_0 and quality factor Q of the BP filter is given by Eqs (10) and (11), respectively:

$$\omega_o = \frac{I_o}{nV_T}\frac{1}{\sqrt{\hat{C}_1\hat{C}_2}} \quad \ldots (10)$$

$$Q = \sqrt{\frac{\hat{C}_1}{\hat{C}_2}} \quad \ldots (11)$$

The realization of the four-quadrant multiplier is shown in Fig. 9. The ouput current of the multiplier is given by Eq. (12):

$$I_{out} = \frac{i_1 . i_2}{I_o} \quad \ldots (12)$$

Thus, if $i_1 = i_2 = i$ the required squarer operation will be obtained.

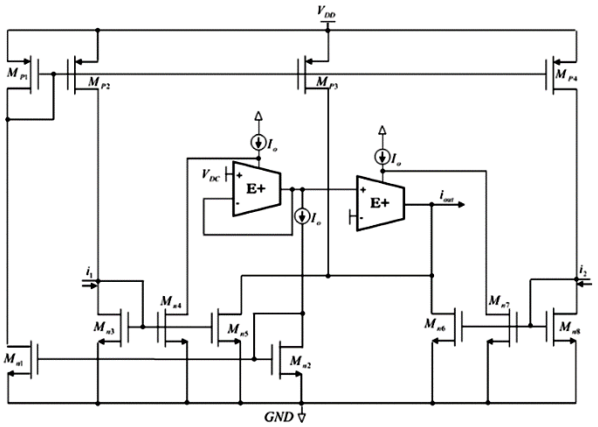

Fig. 9 — Topology of four-quadrant multiplier.

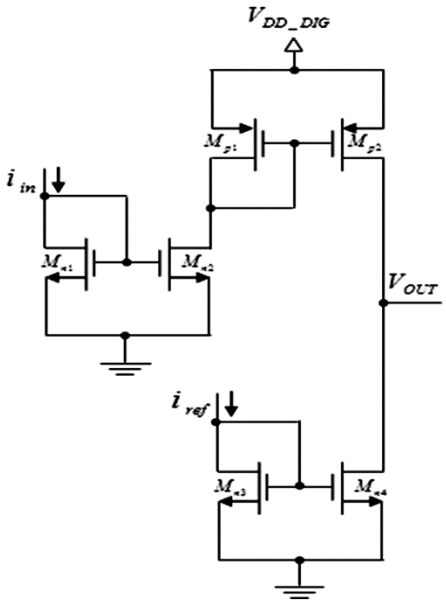

Fig. 10 — MOS implementation of comparator circuit.

Finally, the comparator and AND gate operations required in the system are performed by the circuits given by Figs 10 and 11, respectively.

4 Simulation and Comparison Results

In order to verify the proper functioning of the system, results were obtained in HSPICE software using 130 nm CMOS process file provided by TSMC. The power supply voltages and dc current sources have been chosen as V_{DD} = 0.5 V, V_{DC} =0.2 V and I_o=1.2 nA. The aspect ratios of the MOS transistors used to design transconductance cells of Figs 5 and 6 are given in Table 1. The frequency responses of low-pass and band-pass filters designed for pole/central frequency and quality factor equal to 50 Hz and 2, respectively, are shown in Figs 12(a) and 12(b). The calculated values of capacitors were $\hat{C}_2 = 224\text{pF}$ and $\hat{C}_2 = 56\text{ pF}$. The simulated results for the demonstration of electronic tunability of the filters obtained for I_o equal top 600 pA, 900 pA, 1.2 nA, 1.8 nA and 2.4 nA are shown in Figs 13(a) and 13(b). The linearity of the low-pass filter was evaluated by performing the total harmonic distortion (THD) analysis. The obtained THD plot is shown in Fig. 14. For a THD level equal to 2%, the value of input signal amplitude was equal to 810 pA. Integrating the noise through the pass band of the filter, the rms value of

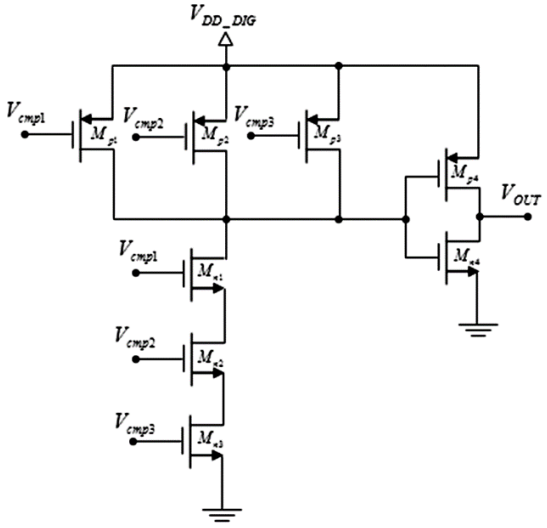

Fig. 11 — MOS implementation of 3-input static AND gate.

Table 1 — MOS transistor aspect ratio for transconductance cell shown in Figs 5(b) and 6(b)

Transistor	*W*/*L* (μm/μm)
Mp1-Mp2	6/5
Mp3	0.5/10
Mn1-Mn4	5/10

the input referred noise was 0.98 pA and the predicted value of the dynamic range (DR) of the filter was 55.33 dB. To study the nonlinear behavior of the band-pass filter, the third-order inter-modulation distortion (IMD3) was measured. For this purpose, a two-tone test was performed using closely spaced tones 49 and 51 Hz (2% of cut-off frequency) that fall within the pass band of the filter. IMD3 response of the filter is drawn in Fig. 15. The noise was integrated over pass-band of the filter and the simulated RMS value of the output noise was 0.54 pA. The achieved DR at 1% distortion level for the filter was 66.2 dB. The sensitivity of the filters to the process parameters variations and MOS transistors parameters mismatching has been evaluated through the employment of the Monte Carlo analysis tools offered by the software. The derived statistical plots for low-pass and band-pass filters are given in Figs 16 and 17, respectively, where the standard deviations of the low frequency gain and pole frequency in case of low-pass filter were 1.47 and 0.577 Hz, respectively, and while the values for maximum pass-band gain and central frequency in case of band-pass filter were 0.91 and 9.1 Hz, respectively.

The output dc characteristics of the four quadrant multiplier of Fig. 8 for i_1 ranging from -800 pA to 800 pA and i_2 as variable input is given in Fig. 18. While as, Fig. 19 shows the ac response of the multiplier operated as squarer for both inputs i_1 and i_2 being sinusoidal signal of 450 pA amplitude. The aspect ratio of the MOS transistors used in multiplier is given in Table 2. Besides, the comparator and logical AND gate blocks have been biased for the supply voltage V_{DD_DIG} =1 V, while the aspect ratios of the MOS transistors used for their design are given in Tables 3 and 4, respectively.

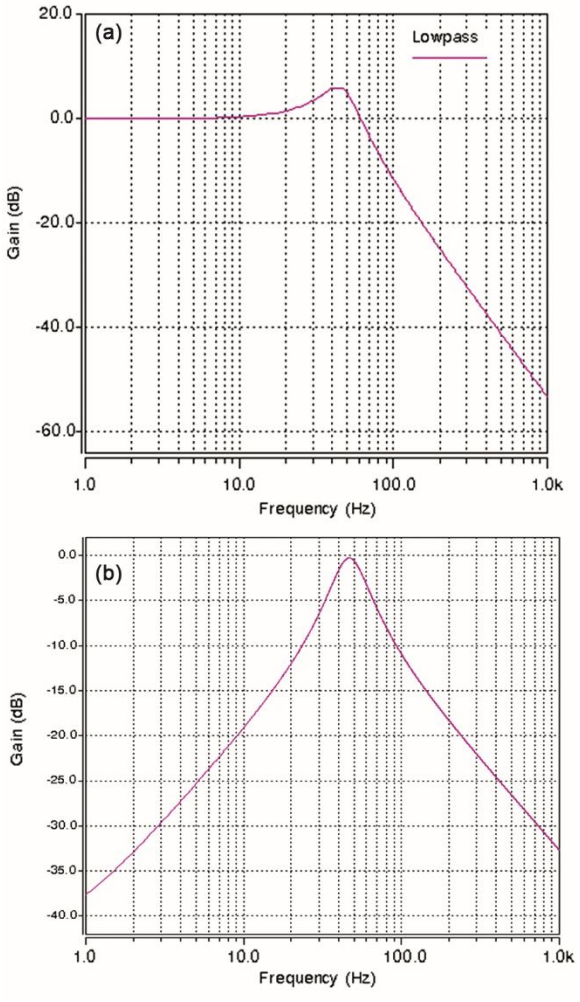

Fig. 12 — (a) Low-pass filter response and (b) band-pass filter response.

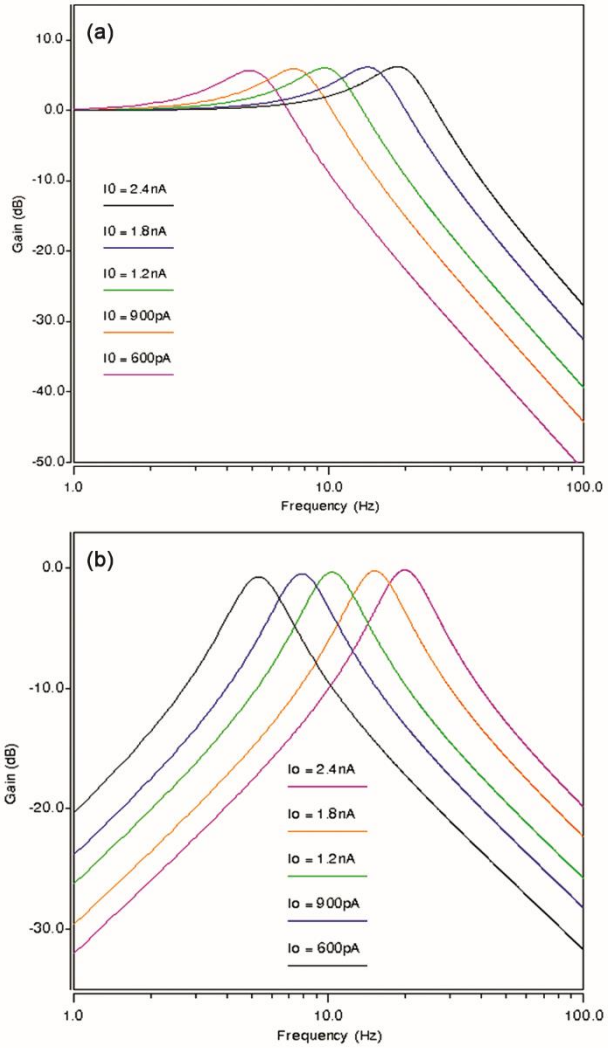

Fig. 13 — Tunability (a) low-pass and (b) band-pass.

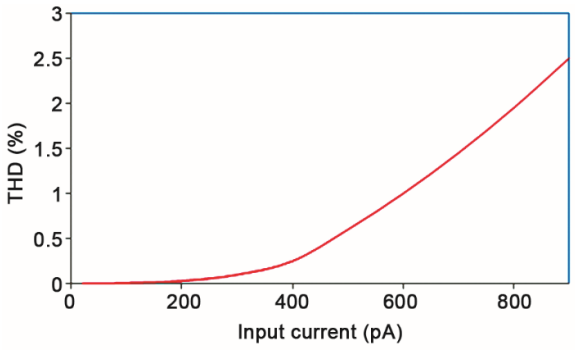

Fig. 14 — THD plot for the low-pass filter.

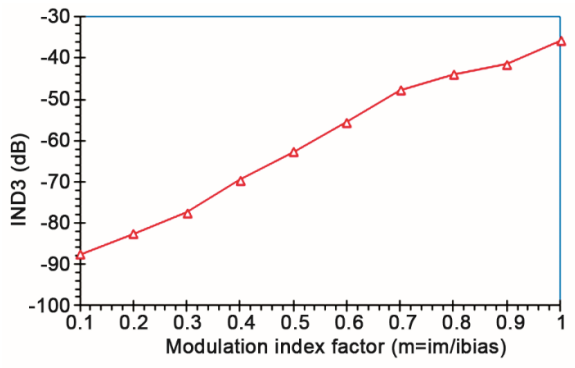

Fig. 15 — IMD3 versus modulation index factor response of band-pass filter.

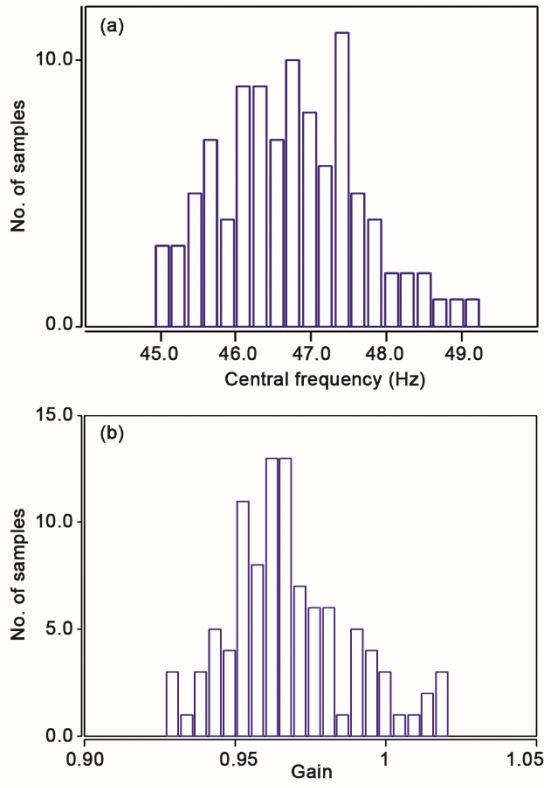

Fig. 16 — Monte Carlo analysis for band-pass filter (a) central frequency and (b) gain.

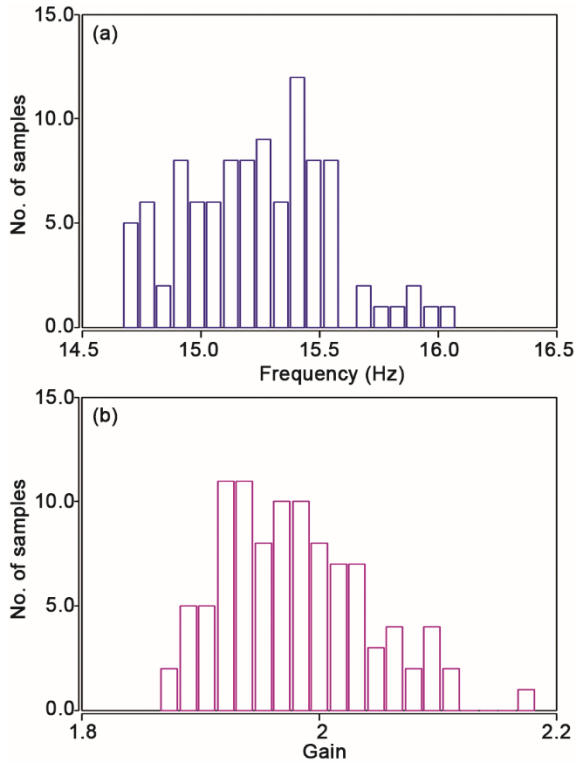

Fig. 17 — Monte Carlo analysis for low-pass filter (a) central frequency and (b) gain.

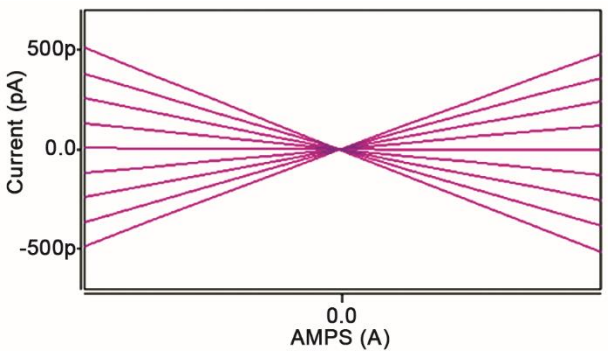

Fig. 18 —DC response of four-quadrant Multiplier.

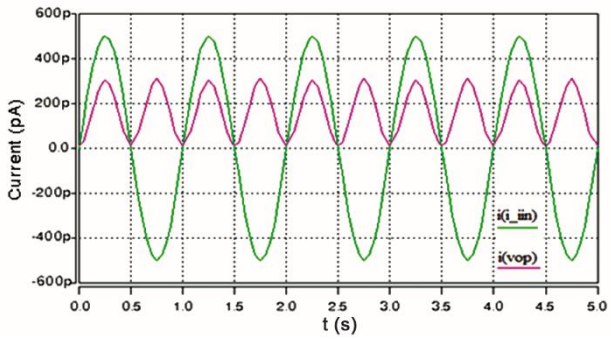

Fig. 19 — Response of multiplier operated as squarer.

Table 2 — MOS transistor aspect ratio for multiplier circuit in Fig. 9

Transistor	*W*/*L* (μm/μm)
Mn1-Mn8	5/10
Mp1-Mn2	1/1

Table 3 — MOS transistor aspect ratio for comparator circuit in Fig. 10

Transistor	*W*/*L* (μm/μm)
Mp1-Mp2	1/1
Mn1-Mn4	5/10

Table 4 — MOS transistor aspect ratio for AND gate circuit in Fig. 11

Transistor	*W*/*L* (μm/μm)
Mn1-Mn3	1.5/0.4
Mn4	10/1
Mp1-Mp3	0.4/0.4
Mp4	3/1

In order to verify the performance of the tinnitus detection system, the alpha, gamma and theta waves were extracted from EEG[27] through appropriate filtering and are shown in Fig. 20(a-c). The alpha, gamma and theta waves in presence of tinnitus are shown in Fig. 21 where the condition $\alpha_1<\alpha_2$, $\Upsilon_1<\Upsilon_2$ and $\theta_1<\theta_2$, has been fulfilled while the corresponding wave in absence of Tinnitus are shown in Fig. 22 where the condition $\alpha_1>\alpha_2$, $\Upsilon_1<\Upsilon_2$ and $\theta_1<\theta_2$ has been fulfilled. The ranges of alpha, gamma, and theta waves are 8–12 Hz, 30–100 Hz, and 4–8 Hz, respectively. Therefore, the values for bias current and capacitor values of the filters within the band energy extractors are given in Tables 5 and 6. The waveforms obtained at the outputs of the corresponding comparators and the output of the whole system in presence of Tinnitus is given in Fig. 23 while the corresponding waveforms in absence of Tinnitus are shown in Fig. 24. As was expected, a logical "1" is observed at the output of the system in presence of Tinnitus while a logical "0" is observed in absence of Tinnitus. The total power dissipation of the system was 1.72 μW. In comparison to the designs proposed by Hiseni *et al.*[7] and Tsirimokou *et al.*[8], the proposed design offers the advantages of low complexity and large dynamic range but the price paid is that the power consumption is large.

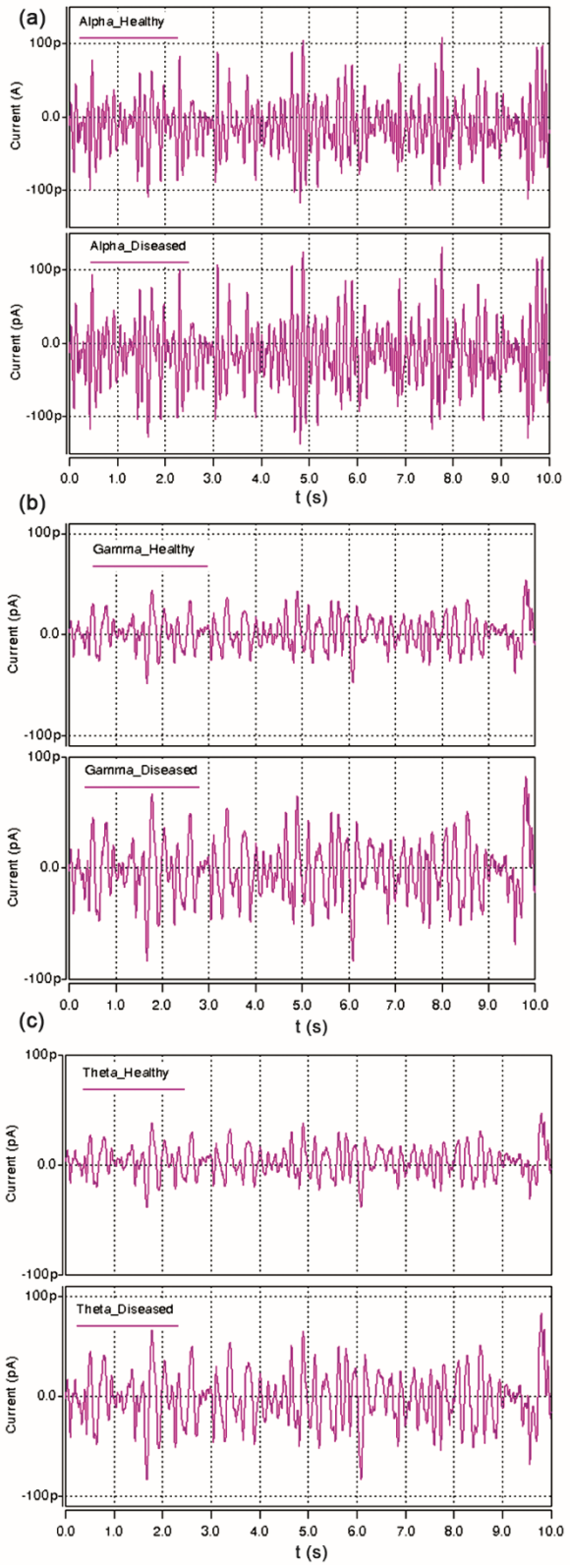

Fig. 20 — Extracted waves (a) alpha wave, (b) gamma wave and (c) theta wave.

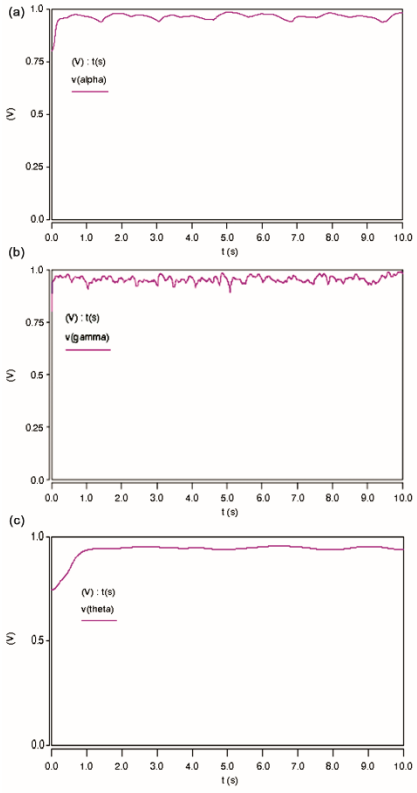

Fig. 21 — Transient response of comparators in presence of Tinnitus (a) alpha, (b) gamma and (c) theta.

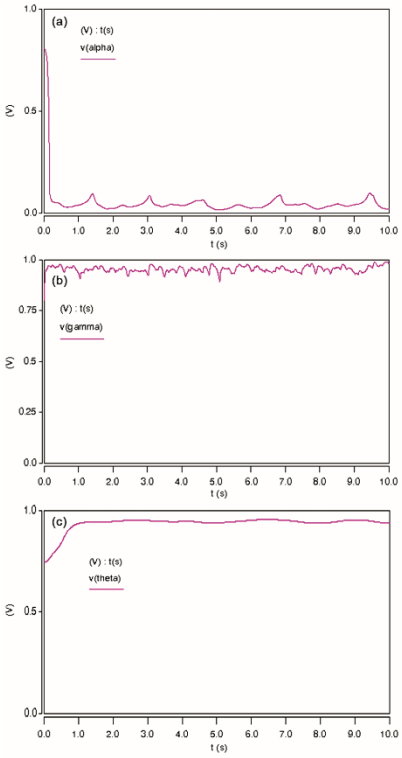

Fig. 22 — Transient response of comparators in absence of Tinnitus (a) alpha, (b) gamma and (c) theta.

Table 5 — Capacitor values for band-pass filter

C_1	C_2	Frequency (actual) (Hz)	Frequency (simulated) (Hz)
2.24×10^{-10}	5.60×10^{-11}	50	48
1.12×10^{-9}	2.80×10^{-10}	10	9.4
2.24×10^{-9}	5.60×10^{-10}	5	5

Table 6 – Capacitor values for low-pass filter

C_1	C_2	Frequency (actual) (Hz)	Frequency (simulated) (Hz)
4.72×10^{-9}	1.18×10^{-9}	2.4	1.91
9.44×10^{-10}	2.35×10^{-10}	12.0	10.00
9.44×10^{-9}	2.35×10^{-9}	1.2	0.97

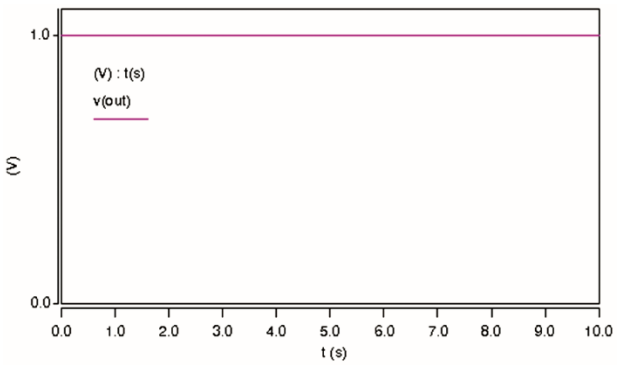

Fig. 23 — Overall response of tinnitus detection system in presence of Tinnitus.

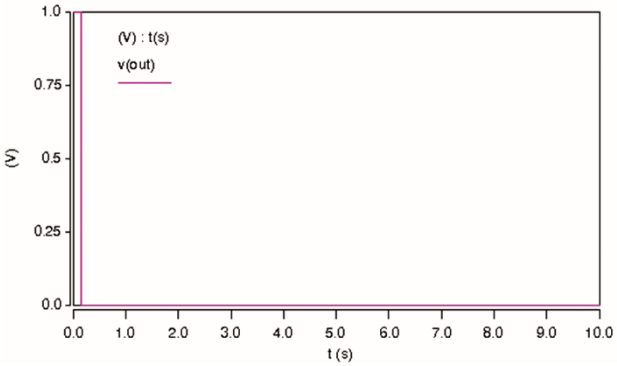

Fig. 24 — Overall response of tinnitus detection system in absence of Tinnitus.

5 Conclusions

In this paper, an ultra-low voltage implementation of the tinnitus detection system is presented. The design is achieved using log-domain companding technique and the proposed implementation has been verified using HSPICE software. The simulation results indicate that the realized tinnitus detection

system with contemporary technology requirements is ready to get applied for its application in biomedical systems.

Acknowledgment

Authors are thankful to the University Grants Commission (UGC), Government of India, under its Special Assistance Programme (SAP) Grant No., F. 3-29/2012(SAP-II).

References

1 Henry J A, Dennis K C & Schechter M A, *J Speech-Lang hearing Res*, 48 (2005) 1204.
2 Folmer R L, Martin W H & Shi Y, *J Family Practice*, 53 (2004) 532.
3 Sindhusake D, Golding M, Wigney D, Newall P, Jakobsen K & Mitchell P, *J Amer Acad Audiol*, 15 (2004) 269.
4 Prusick L, *Multiflex tinnitus technology handbook*, (Starkey), (2015) 9-28.
5 Møller A R, Langguth B, DeRidder D & Kleinjung T, *Textbook of tinnitus*, (Springer), 2011, 9.
6 Snow J B, *Tinnitus: Theory and management*, (PMPH: USA), (2004) 1.
7 Hiseni S, Sawigun C, Vanneste S, van der Velden E, Ridder D & Serdijn W, *Proc IEEE Biomed Circ Syst Conf* (BioCAS), San Diego, CA, (2011) 33–36.
8 Tsirimokou G, Laoudias C & Psychalinos C, *J Low power Electron*, 9 (2013) 458.
9 Tsividis Y, *IEEE Trans Circ Syst-I*, 42 (1995) 561.
10 Tsividis Y, Gopinathan V & Toth L, *Electron Lett*, 26 (1990) 1331.
11 Frey D, *IEE Proc*, Part-G140 (1993) 406.
12 Kontogiannopoulos N & Psychalinos C, *IEEE Trans Circ Syst-I*, 52 (2005) 2043.
13 Shah N A & Khanday F A, *Frequenz*, 68 (2008) 30.
14 Shah N A & Khanday F A, *Frequenz*, 69 (2009) 36.
15 Psychalinos C, *Int J Circuit Theor Appl*, 35 (2007) 17.
16 Haddad S, Bagga S & Serdijn W, *IEEE Trans Circ Syst-I*, 52 (2005) 2013.
17 Stoumpou E, Khanday F A, Psychalinos C & Shah N A, *Analog Integr Circ S*, 61 (2009) 315.
18 Stoumpou E & Psychalinos C, *Int J Circuit Theor Appl*, 39 (2011) 719.
19 Laoudias C, Psychalinos C & Stoumpou E, *Int J Circuit Theor Appl*, 41 (2013) 307.
20 Khanday F A, Psychalinos C & Shah N A, *Int J Electron*, 101 (2014) 894.
21 Kasimis C & Psychalinos C, *Circ Syst Signal Proc*, 31 (2012) 1257.
22 Kafe F & Psychalinos C, *Analog Integr Circ S*, 78 (2014) 217.
23 Psychalinos C & Vlassis S, *IEEE Trans Circ Syst-I*, 49 (2002) 1702.
24 Kasimis C & Psychalinos C, *Int J Circuit Theor Appl*, 40 (2012) 1019.
25 Kasimis C & Psychalinos C, *Int J Electron Comm (AEU)*, 65 (2011) 673.
26 Sawigun C & Serdijn W, *Electron Lett*, 45 (2009) 483.
27 Physio Net web site (PhysioBank ATM) http://www.physionet.org/cgi-bin/atm/ATM.